Paper No.
C2024-21152

AMPP™
ANNUAL CONFERENCE + EXPO
MARCH 3-7, 2024 | NEW ORLEANS, LOUISIANA

# Learning From Failure:
# The Key to Advancements in Metallurgy and Corrosion

Anil Kumar Chikkam, Aaron Ulmer, Edward Larkin, and Mehrooz Zamanzadeh
Matergenics Inc
100 Business Center Dr
Pittsburgh, PA, 15205
USA

## ABSTRACT

In the field of metallurgy and corrosion, it is of paramount importance to acknowledge that no failure should ever be underestimated or dismissed as trivial. Each failure carries its own unique narrative and offers invaluable insights into the underlying causes and potential risks. This paper emphasizes the utmost significance of understanding and analyzing metallurgical failures, irrespective of their perceived severity. By meticulously examining every failure as an individual case, substantial lessons can be derived, leading to advancements in designs, materials, and manufacturing processes. Through meticulous investigations and the application of failure analysis techniques, the intricate stories concealed within each failure can be unraveled. These comprehensive analyses provide crucial information for identifying root causes and establishing preventive measures. The paper presents compelling case studies that exemplify the consequences arising from insufficient knowledge on material selection, neglecting stress raisers, mishandling of materials, and the absence of robust inspection plans. These failures range from production losses to fatal incidents, underscoring the criticality of learning from past experiences and implementing proactive measures to avert such occurrences.

Keywords: failure analysis, metallurgy, corrosion, overheating, stress corrosion cracking, and improper material selection.

## INTRODUCTION

The concept of failure analysis has ancient origins, dating back millennia to the time of the Babylonian King Hammurabi. King Hammurabi realized that poor construction practices led to the tragic loss of human lives and property. His approach to address failure analysis was rooted in the principle of retribution. In cases where someone was responsible for a death, they would face the same fate. If a client's son met an unfortunate end due to negligence, the responsible party's son would also suffer the consequences. Moreover, if a building collapsed due to substandard construction, it was mandated that it be reconstructed without any financial burden placed upon the client.

Failure analysis entails scrutinizing the characteristics and origins of equipment or component failures, involving the examination of physical evidence and the application of engineering and scientific principles and analytical tools. The primary objective is to understand and characterize the causes of failure, with

the ultimate aim of preventing similar failures in the future. However, relying solely on physical evidence may fall short of achieving this goal. The scope of a failure analysis may extend beyond identifying the correctable root cause, often concluding after identifying the failure mechanism and potential causal factors. To ensure a comprehensive understanding and enable the identification of appropriate corrective actions, practitioners may apply root-cause analysis (RCA) principles to ensure a deeper comprehension of the root cause and facilitate the development of effective remedies. [1]

## CASE HISTORY 1:
## UNLOCKING THE ROTOR RIDDLE: CAUSES OF PREMATURE FAILURE

### Introduction

In this instance, a downhole drilling rotor sample that failed prematurely in service was analyzed. In total, two (2) rotors have failed and both rotors had split in 3 places at the box end of the rotor. Visual inspection noted a 15 degree bend in the piston/thrust housing area.

### Test Results

Visual Examination

Figure 1 shows the failed rotor sample. The failed rotor had three longitudinal cracks at the box end of the rotor. The close-up of three cracks were also included in Figure 1. During the examination, several notable findings were made regarding the rotor: deep clamping marks were evident on the outer diameter of the box end, with a diameter measuring approximately 1.8500 inches (46.99 mm). Threads were observed on the inner diameter of the box end, and the observed cracks extended the full length of the threaded section. At a distance of approximately 1.0085 inches from the box end, a reduced diameter, in line with design specifications, was noted, measuring approximately 0.4795 inches, and part identification punching marks were present within this reduced diameter. Additionally, it was observed that the primary crack had propagated along the indentation mark labeled as "1," and noticeable bulging was identified in close proximity to the box end of the rotor.

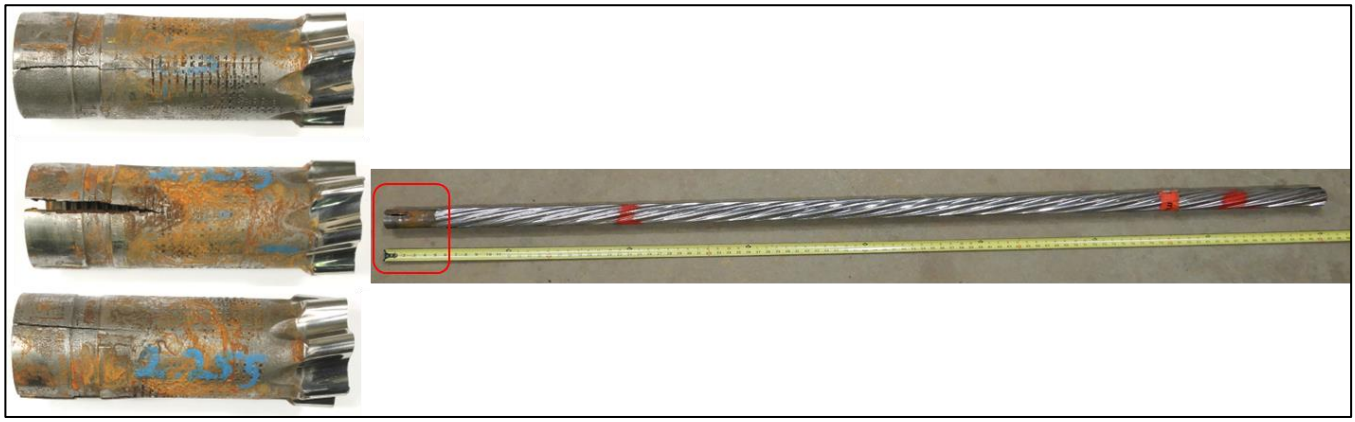

**Figure 1: Photograph of the failed rotor.**

Chemical Analysis

For chemical analysis, a small sample was extracted from the rotor sample and analyzed with an optical emission spectrometer (OES), inductively coupled plasma optical emission spectrometer (ICP-OES) and carbon analyzer. Chemical analysis test results (Table 1) confirm that the material of the rotor does not meet chemistry requirements of ASTM[(1)] A29 [2].

[(1)] ASTM International, 100 Barr Harbor Dr., West Conshohocken, PA 19428-2959.

**Table 1:**
**Chemical Analysis**

| Element | 4140 as per ASTM A29 | | 4142 as per ASTM A29 | | Actual Test Results | Remarks |
|---|---|---|---|---|---|---|
| | Min | Max | Min | Max | | |
| Carbon | 0.38 | 0.43 | 0.40 | 0.45 | 0.43 | Meets Spec |
| Manganese | 0.75 | 1.00 | 0.75 | 1.00 | 1.64 | Does not meet Spec |
| Phosphorous | -- | 0.035 | -- | 0.035 | 0.011 | Meets Spec |
| Sulfur | -- | 0.040 | -- | 0.040 | 0.25 | Does not meet Spec |
| Silicon | 0.15 | 0.35 | 0.15 | 0.35 | 0.28 | Meets Spec |
| Nickel | -- | -- | -- | -- | 0.087 | Meets Spec |
| Chromium | 0.80 | 1.10 | 0.80 | 1.10 | 0.13 | Does not meet Spec |
| Molybdenum | 0.15 | 0.25 | 0.15 | 0.25 | 0.026 | Does not meet Spec |
| Copper | -- | -- | -- | -- | 0.20 | Meets Spec |
| Iron | Balance | | Balance | | 96.92 | Meets Spec |

Metallography

A longitudinal cross-section was extracted from the unaffected area of the box end of the rotor. The cross-section was ground, polished to 1µ surface finish and examined under optical microscope. Optical microscopy of the cross-section in the as-polished condition revealed that the steel is dirty i.e., significant presence of inclusions noticed in the steel. Non-metallic inclusions are undesirable components of all steels because they have adverse effects on the steel properties.

Figure 2 taken at the thread flank close to the thread root showed inclusions in the steel. Figure 3 taken at the reduced diameter showed micro-crack initiation at inclusion. Furthermore, it was observed that the microcrack is following along the MnS Stringer.

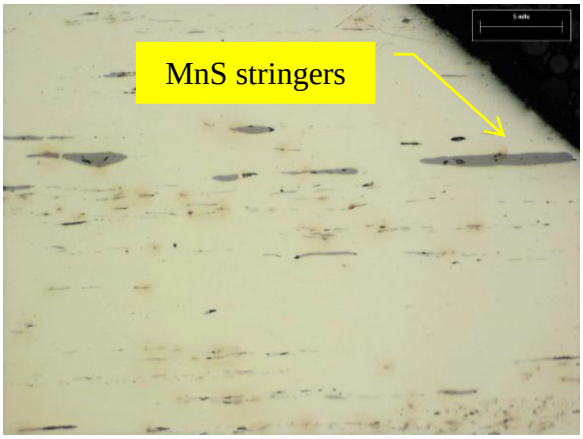


**Figure 2: Photomicrograph taken at one of the thread flanks near thread root showing significant presence of MnS stringers. As polished condition. Magnification: 100X**

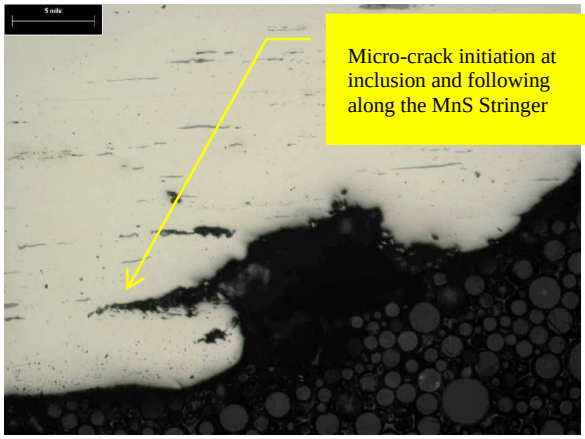


**Figure 3: Photomicrograph taken at the reduced diameter showing micro-crack initiation at inclusion and the microcrack is following along the MnS Stringer. Magnification: 100X.**

As per material specification requirements, the steel must be supplied in quenched and tempered (Q&T) condition. Q&T steel consists of tempered martensitic structure. Microexamination after etching with 2% Nital revealed ferrite and pearlite at the thread flank (Figure 4). A significant presence of MnS stringers was also detected. Figure 5 taken at the reduced diameter showed micro-crack initiation at inclusion and the microcrack is following along the MnS Stringer and bands of ferrite. Microexamination at random

location in the core of the specimen revealed that the overall microstructure of the steel consists of pearlite and bands of ferrite. MnS inclusions are distributed throughout the sample.

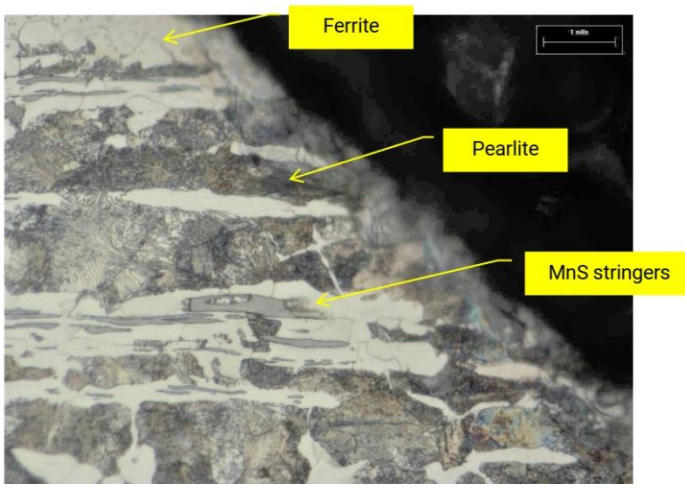


**Figure 4: Photomicrograph taken at one of the thread flanks near thread root showing ferrite and pearlite. Etched with 2% Nital. Magnification: 400X.**

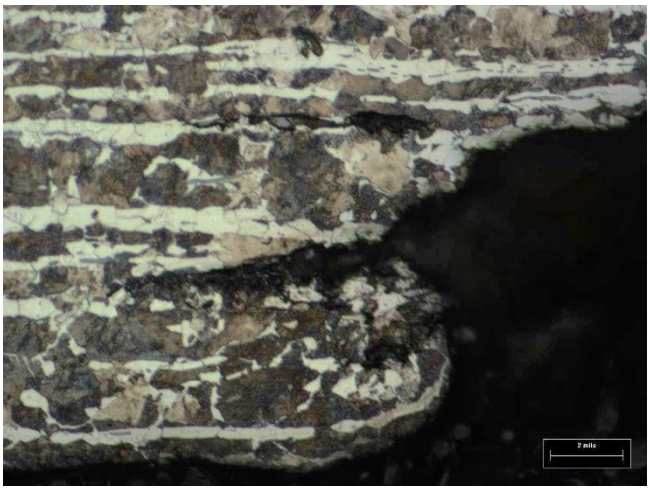

**Figure 5: Photomicrograph taken at the reduced diameter showing micro-crack initiation at inclusion. Etched with 2% Nital. Magnification: 200X.**

Fractography

SEM examination (Figure 6) at the reduced diameter has revealed that the main crack followed along the indentation mark “1”. Reduced diameter and the punching marks in the reduced diameter are stress concentration areas. Figure 7 taken on the fracture surface after ultrasonic cleaning revealed woody overload features. The morphology was identified as predominantly ductile rupture with faint indications of cleavage, and the directionality of the features was suggestive of shear overload. Fracture preferentially followed the nonmetallic inclusions in the longitudinal direction.

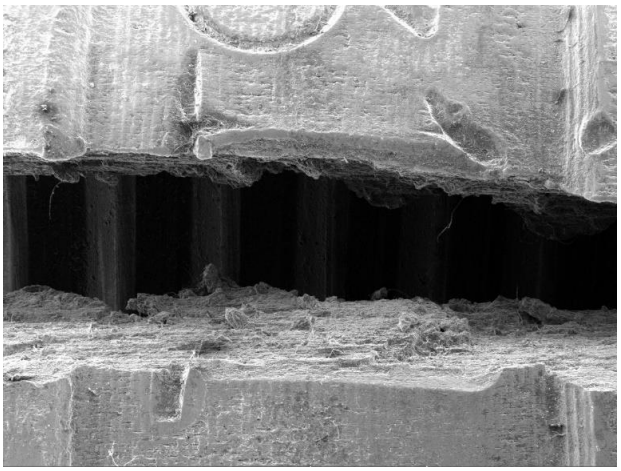

**Figure 6: SEM image showing that the main crack followed along the indentation mark “1”.**

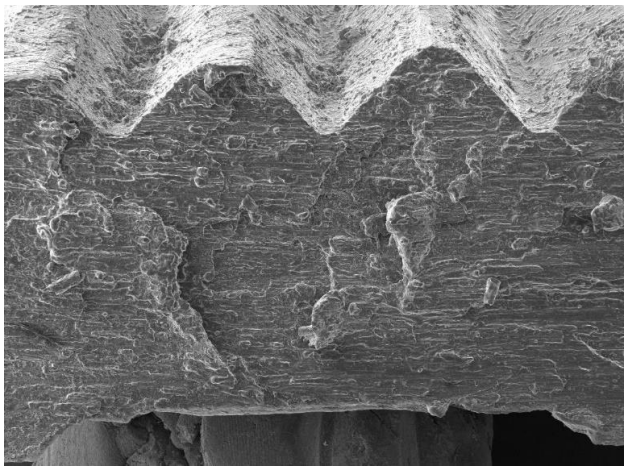

**Figure 7: SEM examination of the fracture surface revealed woody overload features.**

**Conclusions for Case History 1**

The premature failure of the downhole drilling rotor sample was characterized by the presence of three longitudinal cracks at the box end. An analysis of the chemical composition, and heat treatment condition revealed deviations from the material specification requirements, with the steel being identified as

substandard. Microexamination unveiled the presence of significant banding within the ferrite and pearlite microstructure. In conclusion, the box end failure resulted from an overload scenario, with the fracture running parallel to the rolling direction, cutting through manganese sulfide stringers and ferrite bands in the base metal matrix. The root cause of this untimely rotor failure can be attributed to the utilization of incorrect material supplied in an improper heat-treated condition, resulting in mechanical properties inferior to the manufacturer's specified values.

**Recommendations for Case History 1**

- Rotor material should be quenched and tempered to meet the mechanical properties. Portable hardness test is recommended on the remaining rotor samples to confirm that the rotor material is supplied in Q&T condition.
- It is recommended that punching marks should be avoided at reduced diameter.

## CASE HISTORY 2:
## THE GREAT TUBING MIX-UP: HOW UNSUITABLE MATERIAL TURNED UP THE HEAT

**Introduction**

This case study discusses a single tubing sample that encountered premature failure during service. The facility had multiple double block and bleed valves in use, with one experiencing tubing failure while operating at standard conditions of 150 psi (1.03 MPa) and 300°F (149°C). It was noteworthy that despite the manufacturer's classification of the tubing as stainless material, it exhibited magnetic properties and was determined to be low alloy steel through positive material identification (PMI) testing. Notably, the internal surface of the tubing near the rupture appeared smooth, with no indications of internal corrosion.

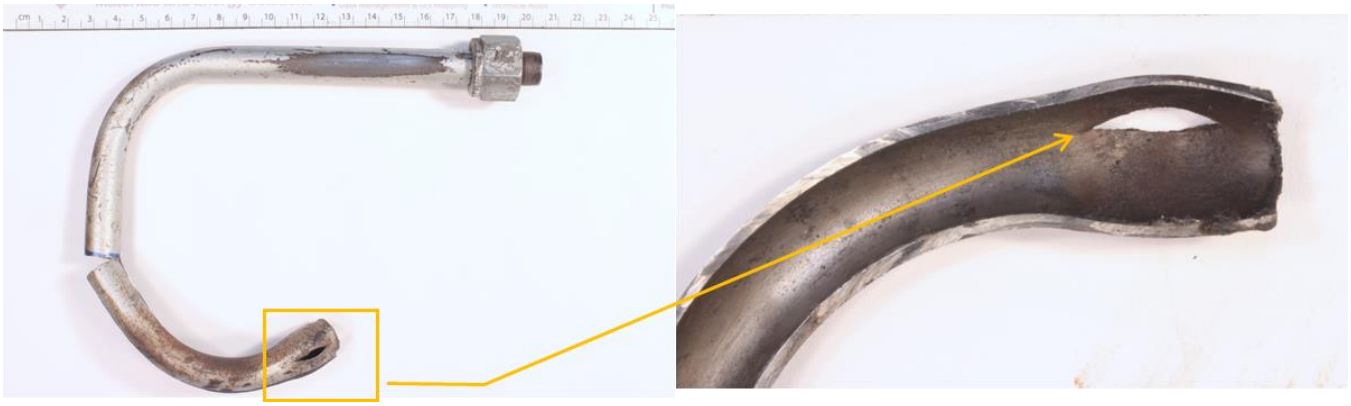

**Figure 8: Photographs showing as received failed tubing. Bulging and wall-thinning at the failed location can be clearly seen.**

**Test Results**

Visual Examination

Figure 8 displays the tubing sample in its as-received state after failure. Visual and Stereoscopic inspection of the failed tubing sample revealed the following physical evidence: the failure exhibited an open burst rupture with noticeable significant bulging and swelling at both the failure site and its neighboring areas. In the vicinity of the rupture, a reduction in wall thickness was observed. Remarkably, no substantial signs of corrosion were detected on either the outer or inner tubing surfaces; however, the inner surface displayed the presence of a black oxide scale.

Hardness Test

To conduct the hardness test, a small sample was taken from the fracture surface of the tubing. Additionally, a transverse cross-section was extracted from an unaffected part of the tubing for comparison. The average Vickers Hardness (HV) measurement was consistent for both the areas that were unaffected and the location of the rupture. Specifically, the unaffected area exhibited a hardness of 177 HV, while the vicinity of the rupture showed a slightly higher value of 185 HV.

Chemical Analysis

For chemical analysis, a small sample was extracted from the unaffected area of the tubing sample and analyzed with an OES, and LECO analyzer. The test results are compared with 304 and 316 stainless steel elemental compositions. Chemical analysis test results (Table 2) confirm that the material of the tubing is carbon steel.

**Table 2:**
**Chemical Analysis**

| **Element** | **SS304** | | **SS316** | | **Actual Test Results** |
|---|---|---|---|---|---|
| | Min | Max | Min | Max | |
| Carbon | -- | 0.08 | -- | 0.08 | 0.11 |
| Manganese | -- | 2.00 | -- | 2.00 | 0.36 |
| Phosphorous | -- | 0.040 | -- | 0.040 | 0.004 |
| Sulfur | -- | 0.030 | -- | 0.030 | 0.007 |
| Silicon | -- | 0.75 | -- | 0.75 | 0.012 |
| Aluminum | -- | -- | -- | -- | 0.050 |
| Nickel | 8.00 | 11.00 | 11.00 | 14.00 | 0.035 |
| Chromium | 18.00 | 20.00 | 16.00 | 18.00 | 0.035 |
| Molybdenum | -- | -- | 2.00 | 3.00 | 0.011 |
| Copper | -- | -- | -- | -- | 0.068 |
| Vanadium | -- | -- | -- | -- | 0.002 |
| Iron | Balance | | Balance | | 99.31 |

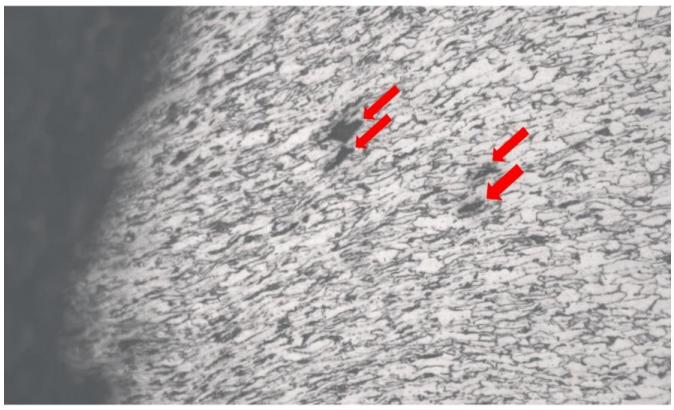

**Figure 9: Elongated grains and the presence of some creep voids (pointed by red arrows) can also be seen. Etched with 2% Nital. Magnification: 200X.**

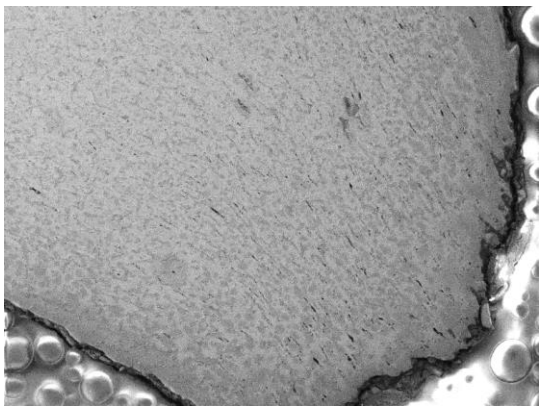

**Figure 10: SEM image showing numerous creep voids (black spots in the material) close to the fracture.**

Metallography

The photomicrograph in Figure 9, taken at the point of rupture, distinctly exhibits elongated grains adjacent to the fracture. Moreover, indications of creep voids are also noticeable. The presence of these microstructural features in proximity to the rupture strongly suggests the occurrence of an overheating phenomenon. The sample was further examined at higher magnifications using SEM. Elongated grains, micro cracks, and creep voids were observed (Figure 10 - 11). The SEM study confirmed the findings from optical microscopy. Regarding the un-deformed grain geometry (Figure 12) in the unaffected area, the grain shape near the fracture displayed an increase in aspect ratio. This suggests material flow under stress at elevated temperatures, leading to bulging and subsequent wall thinning.

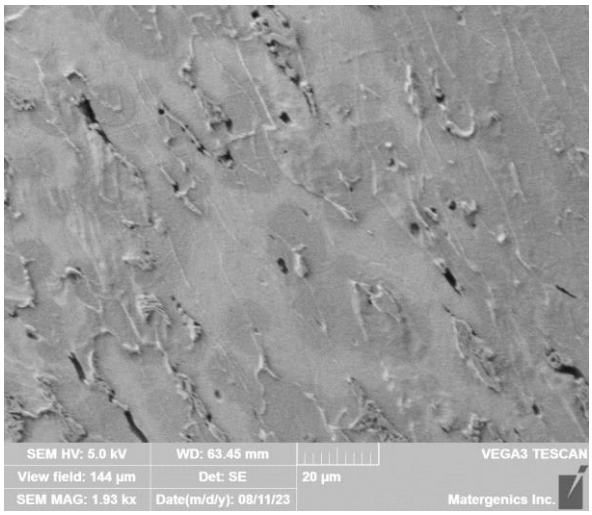


**Figure 11: SEM image showing elongated grains and the presence of some creep voids.**

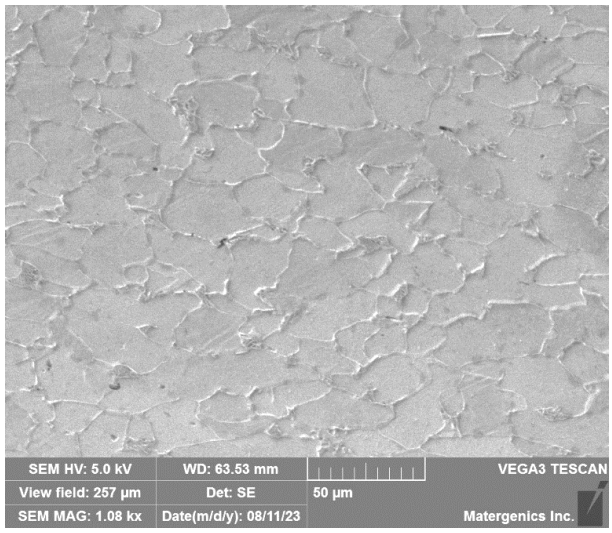


**Figure 12: Figure 10: SEM image taken at the unaffected area.**

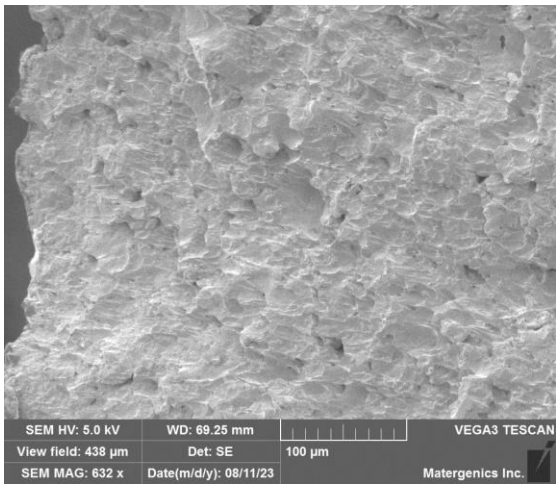


**Figure 13: SEM examination of the fracture surface revealed elongated dimples indicating ductile fracture.**

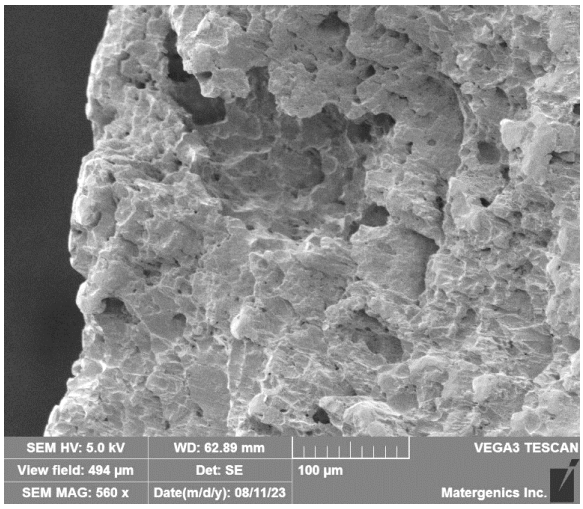


**Figure 14: SEM examination of the fracture surface revealed elongated dimples indicating ductile fracture.**

Fractography

The oxides/deposits were removed from the fracture surface through ultrasonic cleaning in a soap solution. Following this, the fracture surface was examined using SEM. Figures 13 - 14, captured on the fracture surface after ultrasonic cleaning, unveiled characteristics of a dimple fracture. In SEM fractography, these dimples were identified as signs of material softening. The ductile fracture indicated that micro-voids had merged, leading to an overload failure. In such a scenario, creep deformation was accompanied by wall thinning through necking. This weakening of the alloy's strength resulted in dimple rupture. If the sole operating mechanism was creep, the failure would manifest as a thick-lipped fish mouth due to the absence of material flow or deformation to reduce wall thickness.

**Conclusions for Case History 2**

The cracked area of the tubing that failed prematurely in service showed local bulging and thinner tube-wall, indicating a short-term overheating issue. Tests confirmed the tubing is made of low carbon steel, not stainless steel. The material's microstructure consists mainly of pearlite and ferrite. Dark voids near the fracture site suggested creep, while elongated grains indicated high-temperature deformation. Hardness measurements were similar at both unaffected and ruptured areas. The root cause analysis identified localized overheating that led to bulging and subsequent thinning, resulting in a fish mouth rupture. The problem arose from using an unsuitable material. Although the current temperature may be acceptable for stainless steel, it exceeded the limits for low carbon steel.

**Recommendations for Case History 2**

- When selecting tubing material, choose an appropriate option following manufacturer recommendations or consider using a suitable stainless steel material.

## CASE HISTORY 3:
## CORROSION OF STAINLESS STEEL WHICH IS UNDER CATHODIC PROTECTION

**Introduction**

This case study focuses on assessing the condition of an SS material present in the water, equipped with 28 anodes and 14 LED lights, and originally constructed in 1991 using a frame composed of 304 stainless steel (SS). The SS material initially encountered corrosion and weld failures, prompting the installation of sacrificial anodes as an initial remedy. However, since 2017/2018, a concerning trend has emerged, with these anodes deteriorating rapidly and adhering to the installation bolts. This development has raised suspicions of stray current being the primary culprit. In response, a comprehensive risk assessment was conducted to investigate the staining issues, aiming to pinpoint the root cause and provide recommendations for necessary remediation measures.

**Test Results**

Visual Examination

Figures 15 – 18 show images taken during the survey of the SS material. Potential survey showed anode C has higher potential compared to anodes A and B. The native potential of 304 stainless steel in the water is -0.309 V. The polarized potential of 304 stainless steel in the water is -0.755 V. A shift in potential values (difference between polarized and native potentials) of >350 V was observed. The condition of the uncoated SS frame, anodes, face rings of the LED lights, and the coating present on the SS frame bottom was checked in detail. Figure 19 shows the photograph of the coated SS material taken after draining the water. Staining was observed at the interface of the coating and the bare SS frame bottom. Irrespective of presence or absence of LED lights, staining was observed at almost entire interface i.e.,

periphery of the coating (Figures 20). However, the extent of staining is more at and around the locations where LED lights were present.

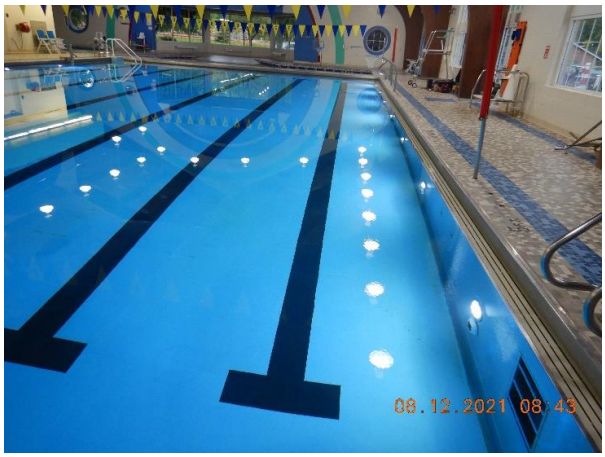


**Figure 15: Photograph showing the SS304 material immersed in the water.**


**Figure 16: Photograph showing the anode A-to-water potential value.**

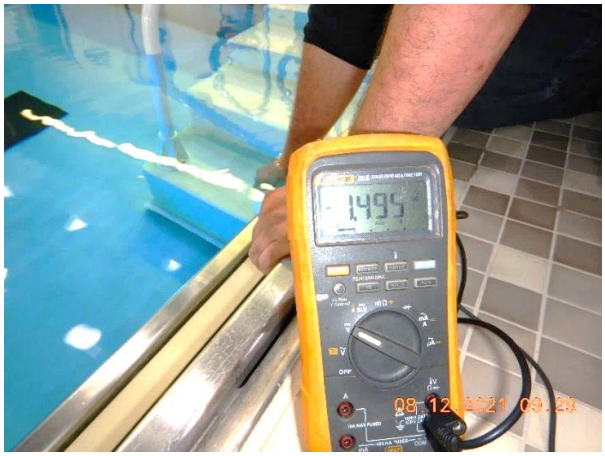


**Figure 17: Photograph showing the anode B-to-water potential value.**

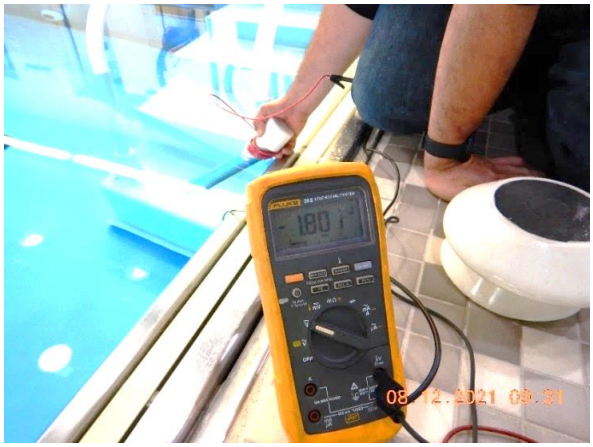


**Figure 18: Photograph showing the anode C-to-water potential value.**


**Figure 19: Photograph showing the condition of the SS material after draining the water.**


**Figure 20: Photograph showing the staining.**


**Figure 21: Photograph showing the condition of anode 2.**


**Figure 22: Photograph showing the condition of anode 4. Corrosion of SS frame behind the anode 4 can be clearly seen.**

The condition of each anode was also checked. Interestingly, almost all anodes are noticeably consumed irrespective of presence or absence of LED lights near the anodes. Figure 21 shows the condition of Anode type A and Figure 22 shows the condition of Anode type B. The condition of remaining Anodes A and B are almost similar as shown in Figures 21 and 22. Figure 22 shows corrosion of SS frame at the contact area of anode 4. Anode 4 was detached, and visual examination was performed. Corrosion of SS frame where anode 4 was in contact with the frame is clearly evident. Closer examination has revealed noticeable pitting and general corrosion attack in the SS frame where anode was in contact with the frame (Figure 23). Further examination was conducted after detaching anode 3. Corrosion of SS frame where anode was in contact with the frame is clearly evident (Figure 24).

**Figure 23: Photograph showing the condition of SS frame where anode 4 was in contact with the frame. Corrosion of SS frame in contact with the rubber of the anode 4 can be clearly seen.**

**Figure 24: Photograph showing the condition of SS frame where anode 3 was in contact with the frame. Corrosion of SS frame in contact with the rubber of the anode 3 can be clearly seen.**

Corrosion of SS frame at the contact area of anodes indicate that the rubber present around the anodes is in contact with the SS frame and it is shielding CP current from entering the contact area and resulting in the corrosion at the contact areas of anodes. It is recommended that the rubber around the anodes should be removed. However, as the rubber is firmly adhered to the anodes, it is recommended to leave a gap such that rubber is not in contact with the SS frame.

During visual examination, it was observed that the SS bolts welded to the SS frame has white deposits (Figure 25) and rust (Figure 26). Presence of deposits or corrosion products on the SS bolts will make detaching old anodes and installing new anodes very difficult. The rust seen on the SS bolt is from the anode lug, and it is seeping into the water and settling at the floor and at the periphery of the coating.


**Figure 25: Photograph showing the condition of SS bolt welded to the frame. Anode 6 is bolted at this location. White deposits can be clearly seen.**


**Figure 26: Photograph showing the condition of SS bolt welded to the frame. Anode 22 is bolted at this location. Presence of rust can be clearly seen.**

**Conclusions for Case History 3**

During the site inspection, PMI analysis was performed on the two newly acquired anodes, designated as Anode A and Anode B. Anode A was unlabeled, while Anode B bore the label "MG 068 PCAP AZ91E." AZ91E denotes a magnesium alloy, with 'A' representing aluminum (Al), 'Z' indicating zinc (Zn), '9' signifying 9% Al, and '1' representing 1% Zn. Surprisingly, PMI analysis revealed that these anodes were not magnesium alloys but rather zinc alloys. Consequently, it was established that the client had received zinc alloy anodes instead of the specified magnesium alloy, and, notably, threads were not directly integrated into the anodes; instead, carbon steel lugs were inserted into the anode.

**Recommendations for Case History 3**

- Connect light protectors to the LED niches.
- Avoid using anodes of different composition. Use anodes of the same material/alloy and from the same supplier to avoid mix-up of anode materials.
- The SS frame bottom should be properly coated without any pinholes. The adhesion of the coating to the SS frame should be strong.
    - The SS material present on the sides is not coated primarily due to esthetic purpose.
    - It is highly recommended that the SS material present on the sides should be coated with different color coating. This will reduce the amount of bare surface to be protected by sacrificial anodes.

## CASE HISTORY 4:
## STRESS CORROSION CRACKING OF SS304 MATERIAL

**Introduction**

In this comprehensive case study, a meticulous exploration of a failed bit is undertaken. The primary objective is to conduct an in-depth analysis to uncover the root cause behind the cracking phenomenon.

## Test Results

Visual Examination

A failed SS304 bit is shown in Figure 27. Closer examination of the bit has revealed multiple cracks far away from the fracture area. Stereoscopic examination of the failed bit has revealed multiple cracks that were not visible to the naked eye (Figure 28). The observed cracks were travelling all along the circumference and not in the axial direction. Figure 29 illustrates EDS test results of the corrosion products present on the fracture surface. From EDS test results, it is evident that Sodium (Na) & Chlorine (Cl) are present in noticeable amounts.

**Figure 27: Photograph showing failed bit.**

**Figure 28: Closer view of the region highlighted in the red box, as shown in figure 27, showing numerous additional cracks other than the visible crack. 7X**

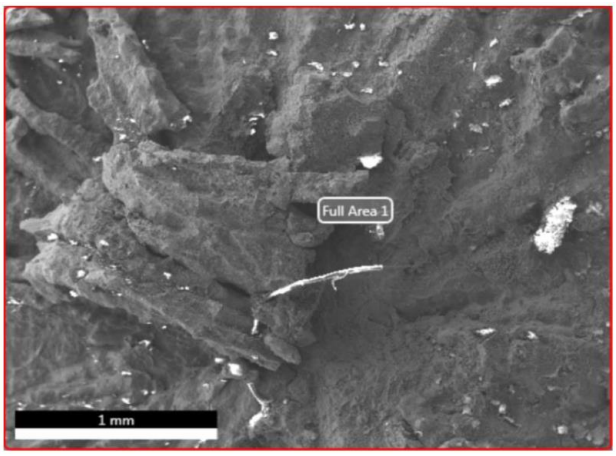


| Element | Weight % | Atomic % |
|---|---|---|
| O K | 24.64 | 51.01 |
| NaK | 3.17 | 4.57 |
| AlK | 0.48 | 0.59 |
| SiK | 0.98 | 1.16 |
| MoL | 0.30 | 0.10 |
| ClK | 1.25 | 1.17 |
| CaK | 0.29 | 0.24 |
| CrK | 9.98 | 6.36 |
| FeK | 54.01 | 32.03 |
| NiK | 4.90 | 2.76 |

**Figure 29: EDS data taken on the fracture surface clearly showing presence of Na, and Cl along with other metal constituents.**

SEM examination of the fracture surface has revealed that the fracture is predominantly intergranular (Figures 30). However, some transgranular fracture was also noticed on the fracture surface but negligible when compared to intergranular fracture region (Figure 31). Microexamination has revealed presence of both surface and sub-surface intergranular cracks (Figure 32). Microexamination after etching with 60% $HNO_3$ & 40% $H_2O$ has revealed that the cracking is predominantly intergranular but transgranular with branching pattern at the tip of the crack (Figure 33).

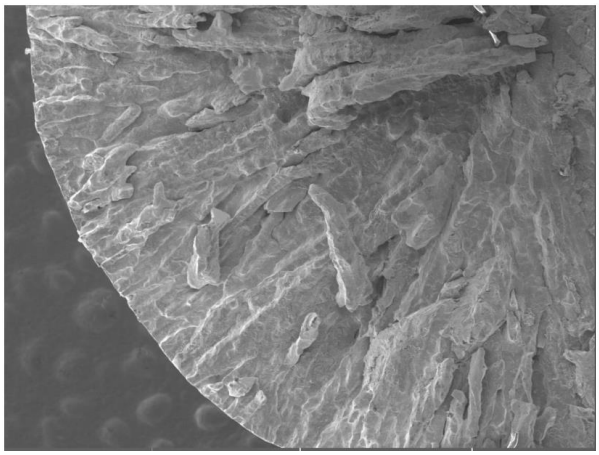

**Figure 30: SEM image of the fracture surface showing intergranular fracture.**

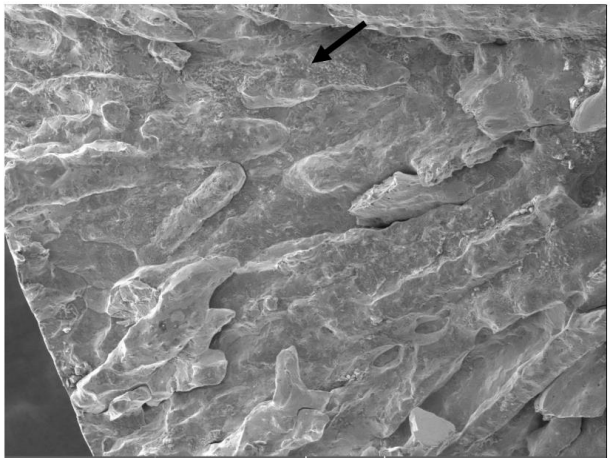

**Figure 31: SEM image of the fracture surface showing predominantly intergranular fracture. Faint indications of transgranular fracture (black arrow) are also noticed.**

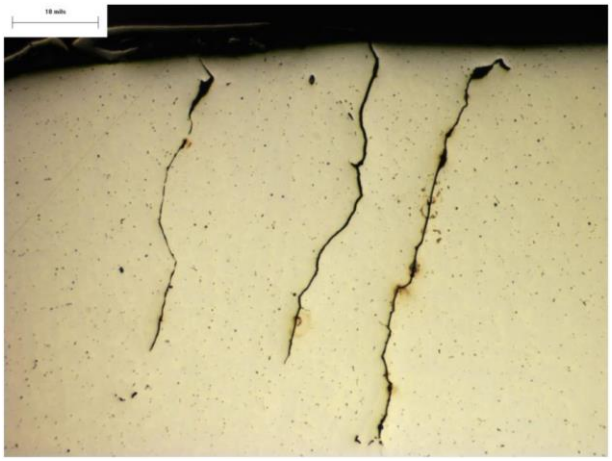

**Figure 32: Photomicrograph showing intergranular cracks at the surface. 50X. As polished condition.**

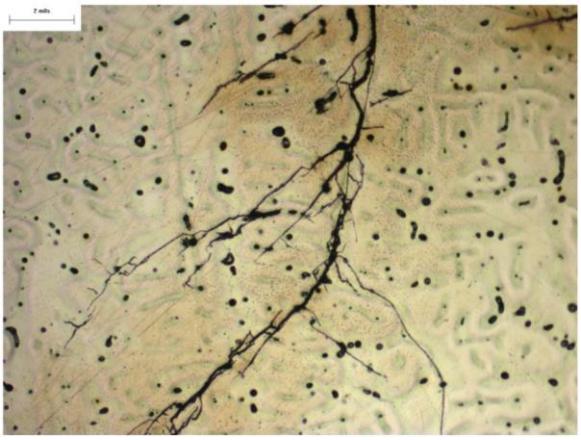

**Figure 33: Photomicrograph showing branching pattern of the crack typical of SCC. 200X. Etched with 60% HNO3 & 40% H2O**

**Conclusions for Case History 4**

In conclusion, the leading factor behind the bit's failure can be ascribed to subpar material quality. Consequently, the progression of cracks was exacerbated by the presence of chlorides. This interaction led to the development of cracks with a branching pattern characteristic of stress corrosion cracking (SCC), representing a secondary contributing factor to the failure.

**Recommendations for Case History 4**

Based on the analysis's conclusion, it's crucial to use high-quality, corrosion-resistant materials in bit production to prevent future failures. Additionally, addressing the impact of chlorides, possibly through specialized coatings or suitable materials, is essential to enhance durability, safety, and performance.

## CONCLUSIONS

In the fields of metallurgy and corrosion, this paper emphasizes the invaluable lessons that failures, regardless of their perceived severity, offer. It underscores the importance of never dismissing failures, as they each hold a unique narrative that can provide insights into underlying causes and potential risks. By subjecting these failures to meticulous examination and utilizing advanced failure analysis techniques, a deeper understanding of their stories can be achieved. These comprehensive analyses are essential for identifying root causes and establishing preventive measures. The paper's case studies vividly illustrate the consequences that can arise from shortcomings in material knowledge, neglecting stress factors, mishandling materials, and inadequate inspection plans, spanning from production losses to catastrophic incidents. These experiences emphasize the necessity of learning from past failures and proactively implementing measures to prevent future occurrences in the ever-evolving fields of metallurgy and corrosion.

## RECOMMENDATIONS

It is strongly recommended that industries involved in metallurgy and corrosion prioritize the practice of failure analysis as an integral component of their operations. Acknowledging the significance of every failure, regardless of its initial perception, can serve as a catalyst for progress, leading to advancements in design, materials, and manufacturing processes. By conducting meticulous investigations and fully embracing the principles of failure analysis, the intricate narratives concealed within each failure can be unraveled, offering valuable insights and lessons. This approach not only contributes to improved safety, reliability, and performance across a broad spectrum of sectors but also encourages a culture of continuous improvement and innovation. Additionally, promoting the adoption of root-cause analysis (RCA) principles is crucial to gaining a deeper understanding of the root causes and facilitating the development of effective remedies when addressing failures. In essence, prioritizing failure analysis and RCA principles fosters a proactive and adaptive approach to mitigating risks and enhancing the resilience of metallurgical and corrosion practices.

## REFERENCES


1. Failure Analysis and Prevention, Volume 11 of ASM [(2)] Handbook.
2. ASTM[(3)] A29/A29M-16, “Standard Specification for General Requirements for Steel Bars, Carbon and Alloy, Hot-Wrought” (West Conshohocken, PA: ASTM).


[(2)] ASM International Materials Park, OH 44073-0002
[(3)] ASTM International, 100 Barr Harbor Dr., West Conshohocken, PA 19428-2959.